








All-laser-microprocessed waveguide Cr:ZnS laser

EVGENI SOROKIN,¹  ANDREY A. BUSHUNOV,^{2,3}  NIKOLAI TOLSTIK,^{4,5} ANDREI A. TESLENKO,^{2,3} ESKIL EINMO,⁴ MIKHAIL K. TARABRIN,^{2,3,6}  VLADIMIR A. LAZAREV,¹  AND IRINA T. SOROKINA^{4,5,*} 

¹Institut für Photonik, TU Wien, Gußhausstraße 27/387, A-1040 Vienna, Austria

²Bauman Moscow State Technical University, Moscow, 105005, Russia

³Novosibirsk State University, Pirogova Str., 2, Novosibirsk, 630090, Russia

⁴Department of Physics, Norwegian University of Science and Technology, N-7491 Trondheim, Norway

⁵ATLA lasers AS, Richard Birkelands vei 2B, N-7034 Trondheim, Norway

⁶P. N. Lebedev Physical Institute of the Russian Academy of Sciences, Moscow, 119991, Russia

*irina.sorokina@ntnu.no

Abstract: We report the proof-of-concept of an operational laser active medium with a depressed cladding waveguide manufactured in the volume of a Cr²⁺:ZnS single-crystalline sample and antireflection microstructures fabricated on its facets exclusively by femtosecond laser processing techniques. This allowed us to achieve transmittance in a broad range from 2 to 8 μm, approaching a maximum of over 90% near 2.5 μm, and lasing at 2275 nm at the average output power of 20 mW for the absorbed pump power of 500 mW with the slope efficiency of 5.5 %. This demonstration opens up a route towards the industrial fabrication of compact integrable laser sources and sensors based on II-VI materials.

© 2022 Optica Publishing Group under the terms of the [Optica Open Access Publishing Agreement](#)

1. Introduction

Transition-metal doped zinc chalcogenides [1,2] and in particular Cr²⁺:ZnS attract a lot of attention from researchers since mid-90s as ultra-broadband and femtosecond [3,4] lasers operating from below 2 to over 3 μm wavelength [5] and capable of delivering the output power in the order of tens of Watts [4]. Based on the demonstrated capabilities and driven by the interest, Cr²⁺-doped II-VI active media have made it to the commercial market, not least because they are very technological in manufacturing and can be successfully used as single crystals and as ceramics, pumped by the fiber and diode lasers [6]. These lasers have found numerous applications, such as sensing [7], spectroscopy [8,9], soft x-ray generation [10], and others. Making a laser or an amplifier active element often requires the elimination of Fresnel reflections on its facets, which can be achieved by antireflection coating (ARC) or placing the medium at Brewster angle. The latter solution, despite its unsurpassed bandwidth, brings issues with elliptical beam shape inside the medium, aggravated by the relatively large refractive index of II-VI semiconductor materials. The more traditional AR coating approach meets the challenge of covering both, the pump and the whole broad gain bandwidth of the Cr²⁺-doped II-VI materials. Also, AR coatings require processing at external facilities with long lead times and are quite expensive unless used in large scale batch manufacturing.

Another solution could be antireflection microstructures (ARMs) which have been demonstrated as a prospective alternative to ARCs for a variety of materials [11,12]. ARM represents micro-sized protrusions or cavities spaced on the sample surface. The antireflection properties are delivered by the fact that incident light of a certain wavelength is smoothly coupled into the bulk of the material, instead of traversing abrupt step in refractive indices between media and substrate [13]. Since this technique is not interferometric, they are broadband by construction. There are

numerous different methods of ARMs fabrication, however, only a few of them are well-suited for the treatment of small-surface areas [12]. Here we demonstrate the application of femtosecond laser direct ablation method for ARMs fabrication on the surface of $\text{Cr}^{2+}:\text{ZnS}$ laser crystal. Laser action in mid-infrared Cr^{2+} -based waveguide active media, fabricated using ultrafast laser processing inside a doped crystal has been demonstrated in polycrystalline $\text{Cr}^{2+}:\text{ZnSe}$ [14], polycrystalline [15] and single-crystalline $\text{Cr}^{2+}:\text{ZnS}$ [16]. Using the ARM to eliminate the Fresnel reflection has also been successfully demonstrated with a bulk $\text{Cr}^{2+}:\text{ZnS}$ laser using the etching techniques [17].

In this work we for the first time use an ultrafast laser processing approach to form both the depressed-cladding waveguide and the ARM surface coating of the laser active medium, thus showing the feasibility of a novel concept of an all-microprocessed waveguide laser – a step forward towards manufacturing a new class of miniature ultra-broadband lasers and sensors.

2. Modeling

There are several key morphological parameters that enable high transmittance through ARM. These are period, depth, filling factor, and cross-sectional profile of ARM [12]. The period determines the spectral region of increased transmittance, whereas the cross-sectional profile defines the effective refractive index gradient and thereby affects the regime of light interaction with the ARM. In this work, ARM with only a smooth profile is discussed, because ARM with step-like profile, also called sub-wavelength microstructures, which acts like a single-layer dielectric coating, is hard to produce with single-pulse femtosecond laser ablation method at current state of the development.

The parameters crucial for maximum transmittance in the discussed case are the depth and filling factor. The average depth of ARM is simply defined as the average size of ARM features in the direction perpendicular to the surface. Generally, the larger the depth, the smoother is the transition between refractive indices of media and substrate, and therefore, the smaller residual Fresnel reflection. The filling factor is defined as a ratio between the treated and untreated area of the surface. If there are a lot of untreated areas between two cavities or protrusions of microstructures, the filling factor is then low and vice versa. The presence of untreated areas produces a step in effective refractive index, therefore leading to residual Fresnel reflection. Minimizing the untreated area, therefore achieving the value of the filling factor closest to 100% is the goal. These assumptions were confirmed with modelling and experimental work in Ref. [12].

In order to obtain a set of microstructure parameters for the most successful $\text{Cr}^{2+}:\text{ZnS}$ crystal blooming in 2–3 μm range, mathematical modeling was carried out using the finite element method. Parameters for optimization were the depth, period, filling factor, and depth profile approximation function. Figure 1 shows the graphs of the dependence of the transmittance on the filling factor and the depth for ARM on ZnS. Figure 1(a) refers to the modeling of the dependence of transmittance on the filling factor, whereas Fig. 1(b) to the modeling of the dependence of transmittance on the depth. For both cases, taking into account the refractive index of ZnS range in the range from 2 to 3 μm , the period of less than 0.8 μm should be chosen. But our method currently has a limit on the minimum hole diameter that can be made, and it is 0.8+ μm . For both simulations cross-section profile was approximated by function $f(r) = r^m$, where r is the distance from the micro-cavity axis and the power m determines the steepness of the cross-section profile approximation function. As shown in previous experiments [18,19], the values of m for the typical laser ablation crater produced by our fabrication setup lie in the range from 2 to 3. We have chosen m equal to 3 for these simulations. The height was fixed at 1 μm for the dependence of the transmittance on the filling factor calculation, while the filling factor was fixed at 0.98 for the dependence of the transmittance on the height calculation.

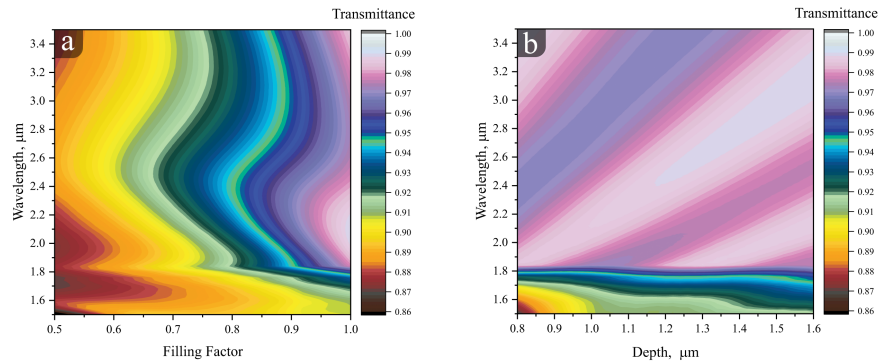


Fig. 1. Modeling of transmittance spectra dependence on height and filling factor of ARM. The depth was fixed at 1 μm for calculation of transmittance dependence on filling factor (a), while the filling factor was fixed at 0.98 for calculation of transmittance dependence on depth (b).

The simulation results have shown that the most successful parameters for creating microstructures in ZnS are follows: the depth of the structure is not less than 1 μm , the filling factor is not less than 90%, the period of the structure is not more than 0.8 μm , and the surface shape function is approximately cubic: $f(r) = r^3$. The simulation results confirm our previous findings that the aspect ratio of 1.1 and above is enough to ensure high transmittance in a desired spectral region.

3. ARM processing

In order to fabricate ARMs, the single-pulse laser ablation method was utilized. The principle of the method is simple and straightforward. The moving sample is irradiated with 200 fs, 513 nm laser pulses at a 20 kHz repetition rate focused with 100 \times , 0.5 NA objective lens, and the laser setup was described in detail in Ref. [18]. Under fs laser irradiation, the material removal happens very locally due to the high energy density of a single fs pulse [20]. The sample movement velocity is chosen so, that the laser pulses impinge on the surface at regular intervals on a one-pulse-per-spot basis, therefore forming an ARM with a certain period. In this work, the aim was to fabricate ARM for 2-3 μm range, therefore we used the period of 0.8 μm as the smallest achievable with the current setup. Average power, focusing depth, and other parameters specified above were optimized during the iterative fabricate-and-test sessions of over 600 samples, covering a wide range of different values. Transmittance in the range from 2 to 10 μm was evaluated using a Lumos FTIR (Bruker) microscope-spectrometer. This device does not allow evacuating the chamber, therefore the atmospheric absorption features are observed in the spectra. The aperture on the surface of the sample was 100 \times 100 μm^2 , the spectral resolution 4 cm^{-1} and the result was averaged over 32 scans.

The best performance with our current fabrication setup [18] is achieved with approximately 150-250 nJ pulse energy and 4 μm focusing depth (the focus is shifted below the substrate surface). Figure 2(a) shows the transmittance spectra of the three ARM samples that have been fabricated in comparison with the untreated ZnS.

The transmittance is less than previously demonstrated for different chalcogenide materials [12,18], due to the insufficient 0.3-0.4 μm depth of the structures and low level of the average filling factor of about 0.8. The shallow structures can be seen on the SEM image made at 45 $^\circ$ (in Fig. 3(a)) and agree with the simulations in Fig. 3(b). The residual material remains pure cubic ZnS and is not subject to stresses or modifications, as can be incurred from the micro-Raman measurement of the processed surface (in Fig. 4). Comparing the Raman spectra

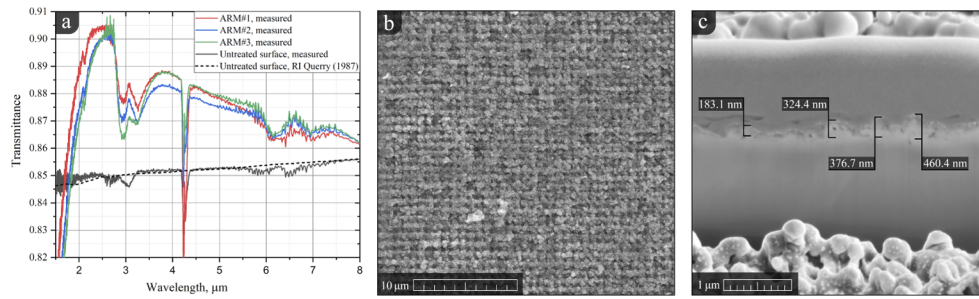


Fig. 2. Transmittance spectra of the ARM samples (a) and SEM images of ARM#1 sample: top-down (b), cross-section profile (c).

of the unprocessed and processed surface, we do not observe any additional lines, that would indicate the existence of ZnO or a different ZnS phase. The only significant spectral change is the enhanced intensity of the LO phonon line at 350 cm^{-1} . Since the relative intensity of this line strongly depends on scattering geometry [21], this enhancement just reflects the fact, that the processed region adds more scattering orientations as compared to the normal incidence on the untreated flat surface.

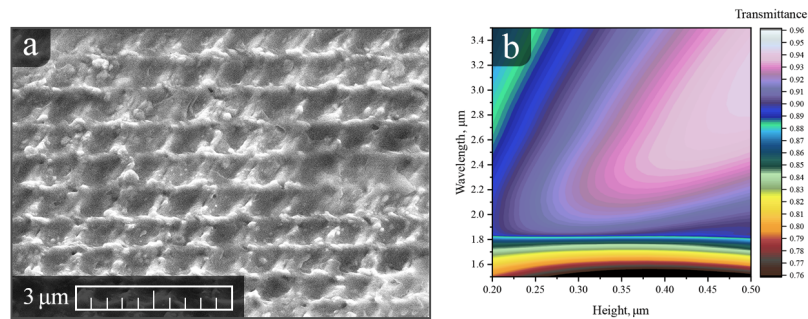


Fig. 3. A 45° SEM image of the ARM structure (a) and transmittance spectra modelling (b) with the actual experimental parameters.

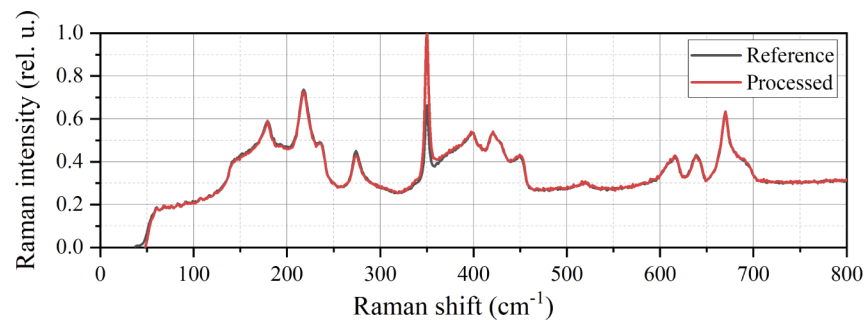


Fig. 4. Micro-Raman spectra of the processed and reference surfaces in unpolarized backscattering geometry.

The low structure depth limits the maximum transmittance of the structures [12]. It is not yet clear, why it was not possible to achieve at least an aspect ratio of 1, as was successfully

demonstrated for other materials [12,18]. This is obviously related to material properties, and a possible guess here is that high sulfur content can affect the ablation dynamics [11,12]. On the one hand, ZnS is more resistant to laser radiation, which significantly reduced the resulting hole depth, and on the other hand, attempts to increase the energy in the pulse led to either a break in the walls between adjacent holes, as shown in Fig. 5(a), or to the formation of cloud-like solidified products of the ablation like shown in Fig. 5(b).

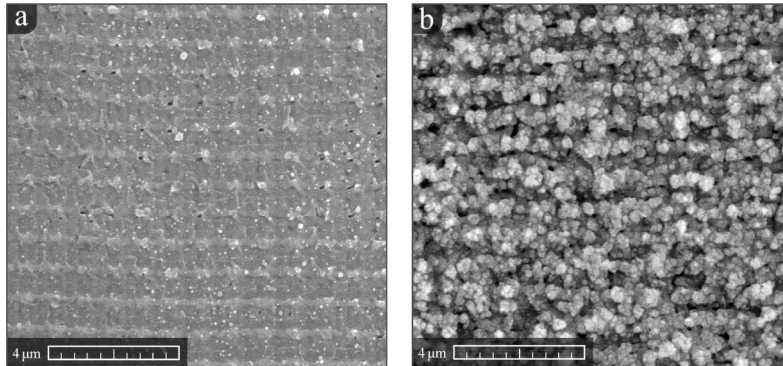


Fig. 5. SEM images of the microstructures made with increased laser energy.

In the first case, a sharp drop in transmittance occurs, since the depth of the microstructures becomes approximately zero. In the second case, microstructures of complex configuration are formed with the presence of a large number of small elements, which significantly increase the scattering. This hypothesis is based on the fact that a similar effect was observed when fabricating ARMs on As_2S_3 [12] and ZnS [11]. We plan an additional investigation, including a close examination of different ARMs fabricated on ZnS and As_2S_3 , as well as chemical element analysis in the ablation zone. The possible solution also may be the utilization of Bessel beams as it was shown in [11].

4. Laser experiments

As a proof-of-principle experiment, we have applied the ARM coating to the front and back facets of the depressed-cladding waveguides manufactured in the volume of a $\text{Cr}^{2+}:\text{ZnS}$ single-crystalline sample. The details about the waveguide manufacturing could be found in [16]. We have ARM-processed the $100 \times 100 \mu\text{m}^2$ sections of the crystal facets, covering the $50 \times 40 \mu\text{m}^2$ waveguide aperture (Fig. 6(a)).

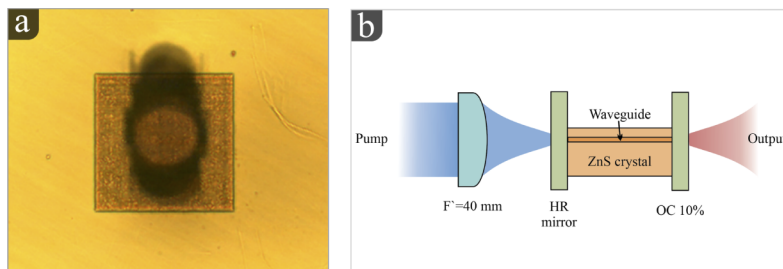


Fig. 6. Microscope image of the depressed cladding waveguide cross-section in $\text{Cr}^{2+}:\text{ZnS}$ with the ARM region covering its facet (a). Laser experiment schematic (b).

The laser experiments were arranged in the plane-parallel laser cavity (Fig. 6(b)), where two dielectric mirrors were mechanically positioned as close as possible to the facets of the waveguide. The pump emission at 1.61 μm from the Er: fiber laser was coupled to the waveguide by a 50-mm focal distance lens AR-coated at 1.5-1.6 μm . The waveguide of 7 mm length with Cr^{2+} concentration about 10^{18} cm^{-3} absorbed about 50 % of the pump emission. The input mirror was highly reflective ($>99.5\%$) for 2.1-2.5 μm and antireflective ($<0.5\%$) for the pump wavelength. The output coupler with 10 % transmittance at the laser wavelength reflected also about 50 % of the unabsorbed pump light. We used the standard-sized 0.5 and 1-inch dielectric mirrors on the fused silica substrates, and with this experimental configuration one has to consider the few micrometer-scale air gaps between the waveguide facets and mirror surfaces, which lead to étalon effects, which could considerably modify the reflectance properties of the cavity mirrors.

The input-output characteristics of the waveguide laser are shown in Fig. 7(a). We reached the average output power of 20 mW for the absorbed pump power value of 500 mW with the slope efficiency of about 5.5 %. This slope efficiency value seems reasonable, given the estimated 0.6 dB propagation losses in the waveguide per pass and residual 10% reflection losses on each surface (Fig. 2(a)), and can be certainly increased by improving the waveguide and ARM coating properties. The emission spectrum is centered at 2275 nm (Fig. 7(b)). It is about 5 nm wide and consists of a number of different lines, which is typical for the case of broadband lasers with parasitic étalons in the cavity.

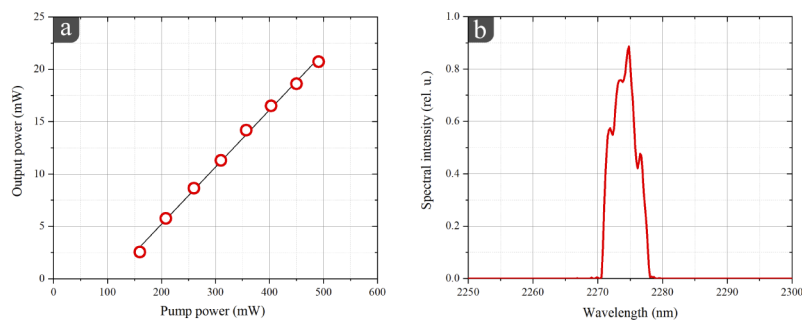


Fig. 7. Output power (a) and optical spectrum (b) of the $\text{Cr}^{2+}:\text{ZnS}$ waveguide laser.

5. Conclusion

We have demonstrated, for the first time to our knowledge, a proof-of-principle of an operational active medium with a direct-written waveguide and antireflection microstructures, fabricated exclusively by ultrafast laser processing techniques. In the future, combining optimized processing and robotic manufacturing technologies, such techniques will allow fabricating active media "on demand" inside an active ion-doped crystals in a single technological process, with software-controlled properties and waveguide geometries.

Funding. Ministry of Science and Higher Education of the Russian Federation (075-15-2021-1008); Norges Forskningsråd (303347); ATLA Lasers AS.

Acknowledgements. AAB, AAT, MKT, and VAL acknowledge the financial support of the Ministry of Science and Higher Education of the Russian Federation grant (Agreement dated 30.09.2021 number 075-15-2021-1008). The work of NT and ITS was supported by NFR project 303347 (UNLOCK) and by ATLA Lasers AS.

Disclosures. NT: ATLA Lasers AS (E). ES: ATLA Lasers AS (I). ITS: ATLA Lasers AS (I,S).

Data availability. Data underlying the results presented in this paper are not publicly available at this time but may be obtained from the authors upon reasonable request.

References

1. L. DeLoach, R. Page, G. Wilke, S. Payne, and W. Krupke, "Transition metal-doped zinc chalcogenides: spectroscopy and laser demonstration of a new class of gain media," *IEEE J. Quantum Electron.* **32**(6), 885–895 (1996).
2. I. T. Sorokina, "Cr²⁺-doped II–VI materials for lasers and nonlinear optics," *Opt. Mater.* **26**(4), 395–412 (2004).
3. I. T. Sorokina and E. Sorokin, "Femtosecond Cr²⁺-based lasers," *IEEE J. Sel. Top. Quantum Electron.* **21**(1), 273–291 (2015).
4. S. B. Mirov, V. V. Fedorov, D. Martyshekin, I. S. Moskalev, M. Mirov, and S. Vasilyev, "Progress in mid-ir lasers based on Cr and Fe-doped II–VI chalcogenides," *IEEE J. Sel. Top. Quantum Electron.* **21**(1), 292–310 (2015).
5. E. Sorokin, I. T. Sorokina, M. Mirov, V. Fedorov, I. Moskalev, and S. Mirov, "Ultrabroad continuous-wave tuning of ceramic Cr:ZnSe and Cr:ZnS lasers," in *Lasers, Sources and Related Photonic Devices* (Optical Society of America, 2010), p. AMC2, <https://doi.org/10.1364/ASSP.2010.AMC2>.
6. I. T. Sorokina, E. Sorokin, S. Mirov, V. Fedorov, V. Badikov, V. Panyutin, and K. I. Schaffers, "Broadly tunable compact continuous-wave Cr²⁺:ZnS laser," *Opt. Lett.* **27**(12), 1040–1042 (2002).
7. C. Fischer, E. Sorokin, I. T. Sorokina, and M. W. Sigrist, "Photoacoustic monitoring of gases using a novel laser source tunable around 2.5 μm," *Opt. Lasers Eng.* **43**(3-5), 573–582 (2005).
8. E. Sorokin, I. T. Sorokina, J. Mandon, G. Guelachvili, and N. Picqué, "Sensitive multiplex spectroscopy in the molecular fingerprint 2.4 μm region with a Cr²⁺:ZnSe femtosecond laser," *Opt. Express* **15**(25), 16540–16545 (2007).
9. B. Bernhardt, E. Sorokin, P. Jacquet, R. Thon, T. Becker, I. T. Sorokina, N. Picqué, and T. W. Hänsch, "Mid-infrared dual-comb spectroscopy with 2.4 μm Cr²⁺:ZnSe femtosecond lasers," *Appl. Phys. B* **100**, 3–8 (2010).
10. V. E. Leshchenko, B. K. Talbert, Y. H. Lai, S. Li, Y. Tang, S. J. Hageman, G. Smith, P. Agostini, L. F. DiMauro, and C. I. Blaga, "High-power few-cycle Cr:ZnSe mid-infrared source for attosecond soft x-ray physics," *Optica* **7**(8), 981–988 (2020).
11. X. Li, M. Li, H. Liu, and Y. Guo, "Fabrication of an anti-reflective microstructure on ZnS by femtosecond laser beam," *Molecules* **26**(14), 4278 (2021).
12. A. A. Bushunov, M. K. Tarabrin, and V. A. Lazarev, "Review of surface modification technologies for mid-infrared antireflection microstructures fabrication," *Laser Photonics Rev.* **15**(5), 2000202 (2021).
13. L. Rayleigh, "On reflection of vibrations at the confines of two media between which the transition is gradual," *Proc. Lond. Math. Soc.* **s1-11**(1), 51–56 (1879).
14. J. R. Macdonald, S. J. Beecher, P. A. Berry, G. Brown, K. L. Schepler, and A. K. Kar, "Efficient mid-infrared Cr:ZnSe channel waveguide laser operating at 2486 nm," *Opt. Lett.* **38**(13), 2194–2196 (2013).
15. J. R. Macdonald, S. J. Beecher, A. Lancaster, P. A. Berry, K. L. Schepler, S. B. Mirov, and A. K. Kar, "Compact Cr:ZnS channel waveguide laser operating at 2333 nm," *Opt. Express* **22**(6), 7052–7057 (2014).
16. N. Tolstik, A. Okhrimchuk, M. Smayev, V. Likhov, E. Sorokin, and I. Sorokina, "Single-mode depressed cladding buried waveguide laser based on single-crystal Cr:ZnS," in *CLEO: Science and Innovations* (to be submitted to Opt. Express) (Optical Society of America, 2019), pp. STh1E–6, https://doi.org/10.1364/CLEO_SI.2019.STh1E.6.
17. S. McDaniel, D. Hobbs, B. MacLeod, E. Sabatino, P. Berry, K. Schepler, W. Mitchell, and G. Cook, "Cr:ZnSe laser incorporating anti-reflection microstructures exhibiting low-loss, damage-resistant lasing at near quantum limit efficiency," *Opt. Mater. Express* **4**(11), 2225–2232 (2014).
18. A. A. Bushunov, A. A. Teslenko, M. K. Tarabrin, V. A. Lazarev, L. I. Isaenko, A. P. Eliseev, and S. I. Lobanov, "Fabrication of antireflection microstructures on the surface of GaSe crystal by single-pulse femtosecond laser ablation," *Opt. Lett.* **45**(21), 5994–5997 (2020).
19. A. A. Bushunov, M. K. Tarabrin, V. A. Lazarev, V. E. Karasik, Y. V. Korostelin, M. P. Frolov, Y. K. Skasyrsky, and V. I. Kozlovsky, "Fabrication of anti-reflective microstructures on chalcogenide crystals by femtosecond laser ablation," *Opt. Mater. Express* **9**(4), 1689–1697 (2019).
20. P. Balling and J. Schou, "Femtosecond-laser ablation dynamics of dielectrics: basics and applications for thin films," *Rep. Prog. Phys.* **76**(3), 036502 (2013).
21. W. G. Nilsen, "Raman spectrum of cubic ZnS," *Phys. Rev.* **182**(3), 838–850 (1969).